Electronic Supplementary Material (ESI) for Dalton Transactions.

Experimental Section

Synthesis of Mo_2C/RGO

All the chemicals were used as received without further purification. Briefly, 0.36 g of GO was ultrasonically dispersed in 100 mL of distilled water to form a homogeneous GO suspension. Then 0.2 g $(NH_4)_6Mo_7O_{24}\cdot4H_2O$ was added in GO suspension under ultrasonication for 30 min. After drying the mixed solution at 80 °C for 24 h, the resulting solid powders were annealed in a tube furnace at 800 °C for 2 h under Ar atmosphere, obtaining Mo_2C/RGO.

Electrochemical measurements

Electrochemical measurement was carried out on a CHI-660E electrochemical workstation. Mo_2C/RGO coated on carbon cloth (1×1 cm^2, 0.5 mg cm^{-2}), Hg/HgO and platinum foil were used as working, reference and counter electrodes, respectively. All potentials reported in this work were referenced to reversible hydrogen electrode (RHE) scale by $E_{RHE} = E_{Hg/HgO} + (0.098 + 0.0591 \times pH)$. The NRA measurements were conducted in Ar-saturated 0.5 M Na_2SO_4 + 0.1 M $NaNO_3$ electrolyte (pH=6.9) using an H-type two-compartment electrochemical cell separated by a Nafion 211 membrane. The Nafion membrane was pretreated by heating it in 5% H_2O_2 aqueous solution at 80 °C for 1 h and then in deionized water at 80 °C for another 1 h. Before NRA test, linear sweep voltammetry (LSV) curves were conducted until that the polarization curves achieve steady-state ones at a rate of 10 mV s^{-1} from 0 to -0.8 V vs. RHE. Then, the potentiostatic test was carried out at different potentials for 1 h, produced NH_3 and other possible by-products were analyzed by various colorimetric methods using UV-vis absorbance spectrophotometer (MAPADA P5). The detailed determination procedures are given in our previous publications [1].

Calculations of NH_3 yield and Faradaic efficiency

$$NH_3\ \text{yield} = (c \times V) / (17 \times t \times A) \qquad (1)$$

Faradaic efficiency was calculated by the following equation:

$$FE = (8 \times F \times c \times V) / (17 \times Q) \times 100\% \qquad (2)$$

where c (μg mL^{-1}) is the measured NH_3 concentration, V (mL) is the volume of electrolyte in the cathode chamber, *t* (s) is the electrolysis time and *A* is the surface area of CC (1×1 cm^2), *F* (96500 C mol^{-1}) is the Faraday constant, *Q* (C) is the total quantity of applied electricity.

Characterizations

Transmission electron microscopy (TEM), selected area electron diffraction (SAED) and high-resolution transmission electron microscopy (HRTEM) were recorded on a Tecnai G^2 F20 microscope. X-ray diffraction (XRD) was conducted on a Rigaku D/max 2400 diffractometer. X-ray photoelectron spectroscopy (XPS) analysis was collected on a PHI 5702 spectrometer. UV-vis absorption spectra were measured on MAPADA ULM 1912006 UV-vis spectrophotometer.

Calculation details

DFT computations were conducted by using Cambridge sequential total energy package (CASTEP). The generalized gradient approximation (GGA) with the Perdew–Burke–Ernzerhof (PBE) exchange-correlation function was utilized in the calculations. The 3×3×1 Monkhorst-Pack mesh was used in Brillouin zone sampling. The convergence tolerance was set as 1.0×10^{-5} eV for energy and 0.02 eV $Å^{-1}$ for force to ensure all atoms were fully relaxed for each system. The kinetic cutoff energy for the plane wave basis was set at 420 eV. The Mo_2C (002) slab was constructed by a 4×4 supercell and a vacuum region of 15 Å was used to separate adjacent slabs. The Gibbs free energy (ΔG, 298 K) of reaction steps is calculated by [2]:

$$\Delta G = \Delta E + \Delta ZPE - T\Delta S \tag{3}$$

where ΔE is the adsorption energy, ΔZPE is the zero point energy difference and $T\Delta S$ is the entropy difference between the gas phase and adsorbed state. The entropies of free gases were acquired from the NIST database.

Molecular dynamics (MD) simulations were carried out using a force field type of universal[3]. The non-bond interaction was processed by Ewald with accuracy of 1.0×10^{-5} Kcal/mol and the repulsive cutoff was chosen as 15 Å. The electrolyte systems were constructed by cubic cells with randomly filling 2000 H_2O, 50 NO_3^- and 50 H^+. After geometry optimization, the MD simulations were performed under the universal field with the total simulation time of 1 ns at a time step of 1 fs.

The radial distribution function (RDF) is calculated as

$$g(r)=\frac{dN}{4\pi\rho r^2 dr} \tag{4}$$

where dN is the amount of particle NO_3^- or H^+ in the shell between the central particle r and $r+dr$, ρ is the number density of NO_3^- or H^+.

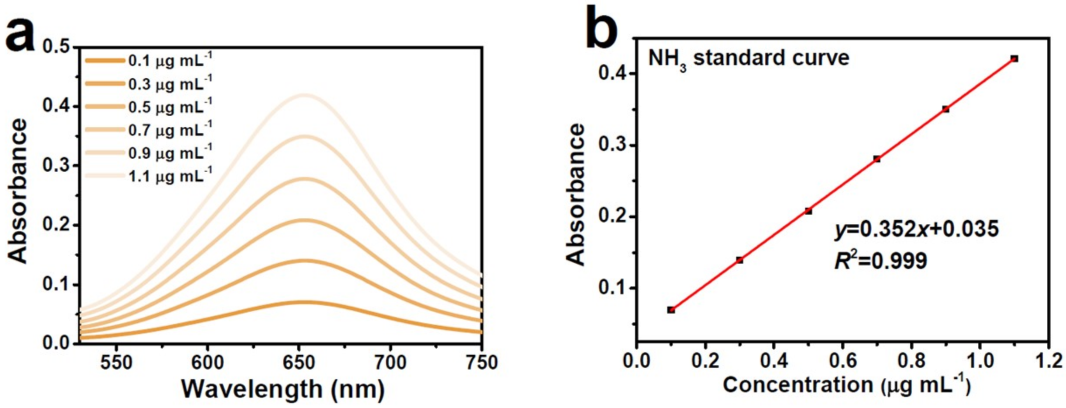

Fig. S1. (a) UV-vis absorption spectra of NH_4^+ assays after incubated for 2 h at ambient conditions. (b) Calibration curve used for the calculation of NH_3 concentrations.

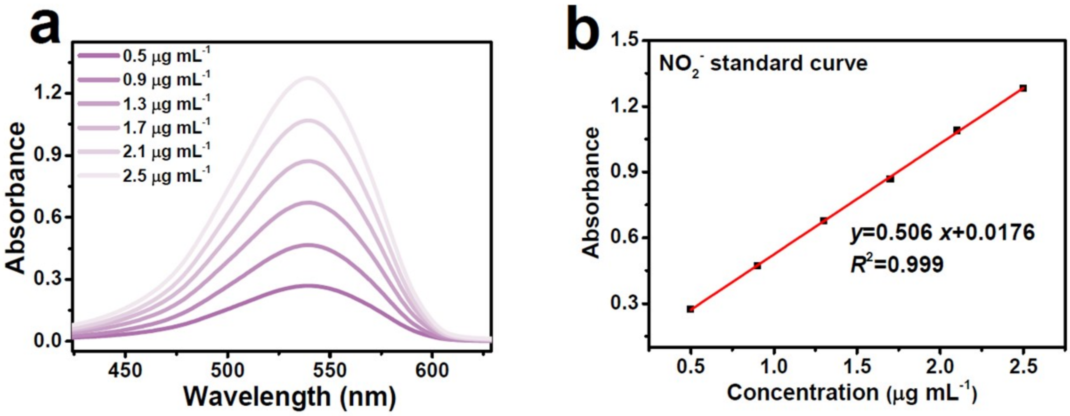

Fig. S2. (a) UV-vis absorption spectra of NO_2^- assays after incubated for 20 min at ambient conditions. (b) Calibration curve used for calculation of NO_2^- concentrations.

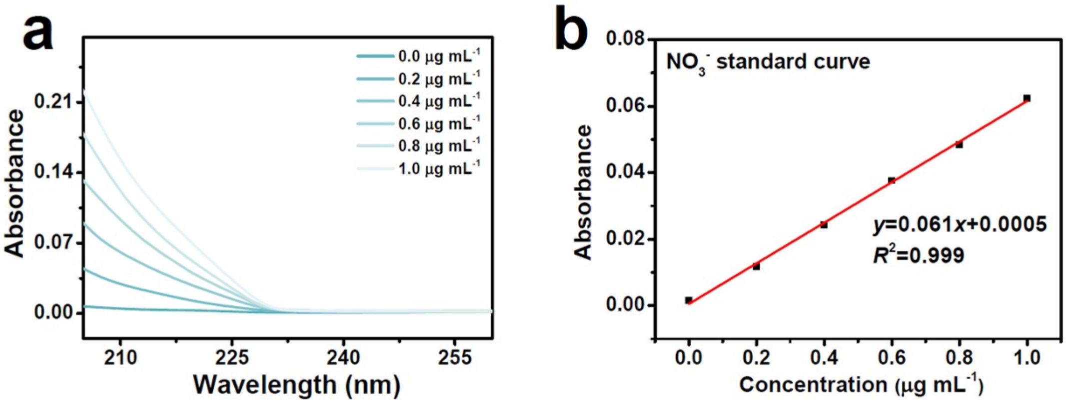

Fig. S3. (a) UV-vis absorption spectra of NO_3^- assays after incubated for 20 min at ambient conditions. (b) Calibration curve used for calculation of NO_3^- concentrations.

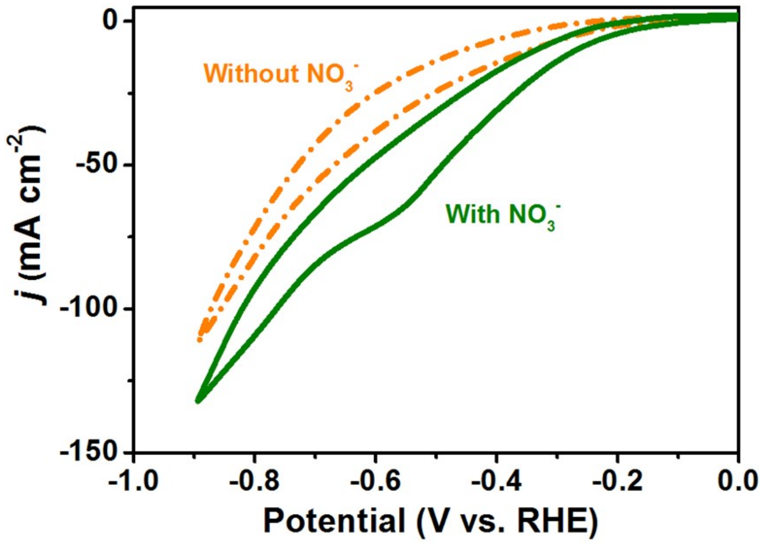

Fig. S4. CV curves of Mo_2C/RGO with and without NO_3^-.

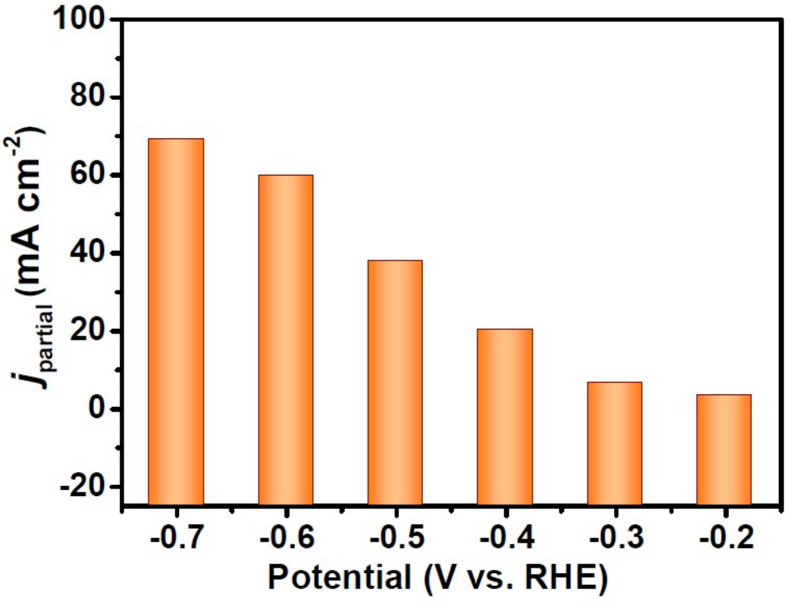

Fig. S5. NH_3 partial current densities of Mo_2C/RGO at various potentials.

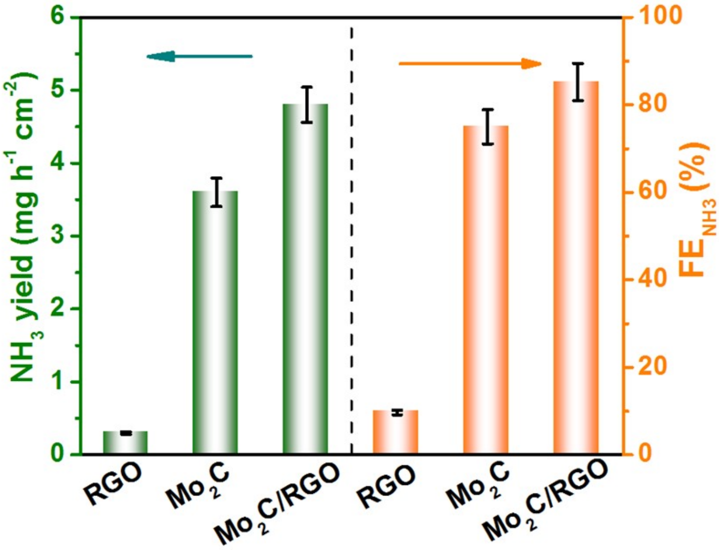

Fig. S6. NH_3 yields and FE_{NH3} of RGO, bare Mo_2C and Mo_2C/RGO at -0.6 V.

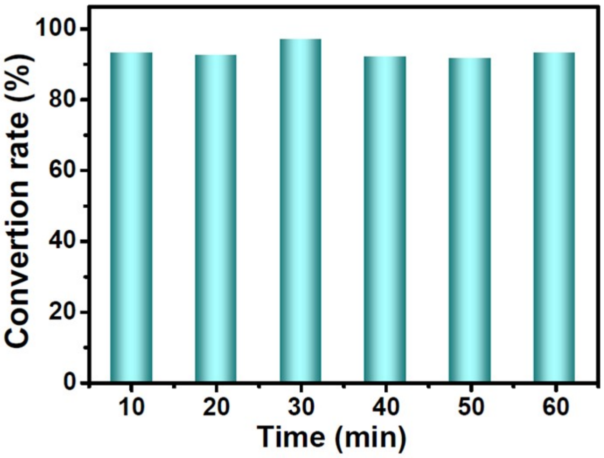

Fig. S7. NO_3^--to-NH_3 conversion rates over Mo_2C/RGO at various electrolysis times at -0.6 V.

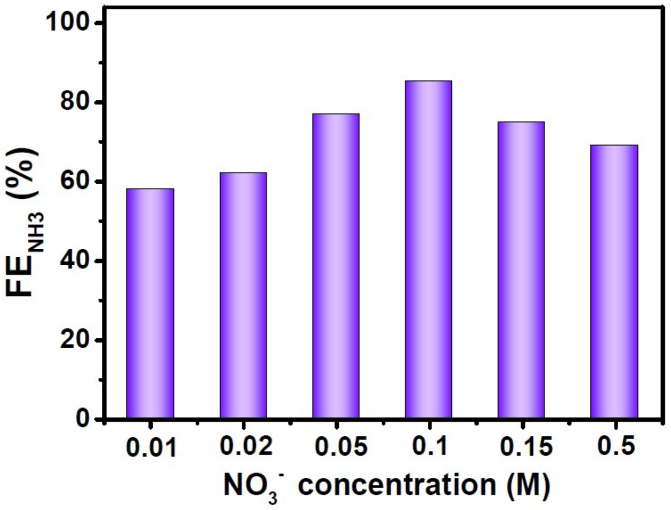

Fig. S8. FE_{NH3} of Mo_2C/RGO at various starting NO_3^- concentrations.

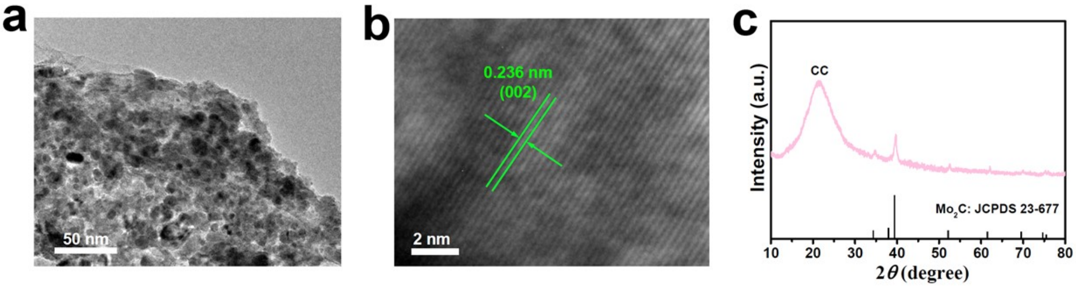

Fig. S9. (a) TEM image, (b) HRTEM image, and (c) XRD pattern of Mo_2C/RGO after stability tests.

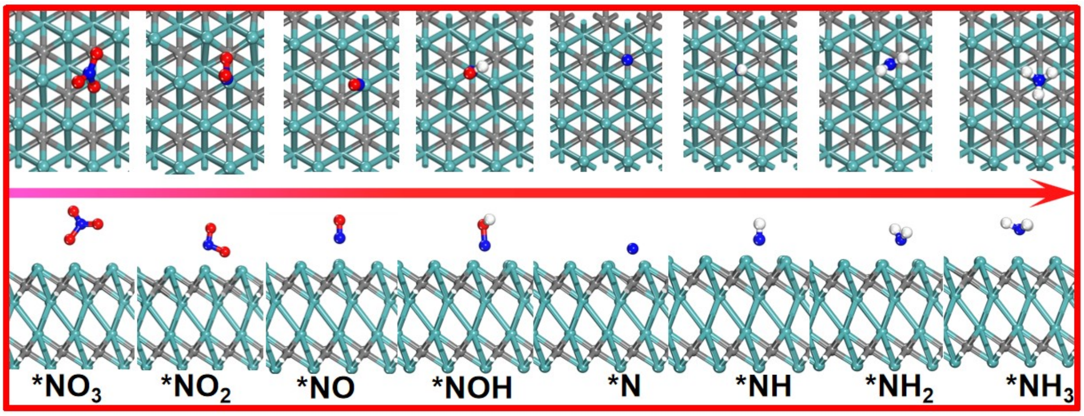

Fig. S10. Optimized structures of intermediate configurations through NOH hydrogenation pathway on Mo_2C.

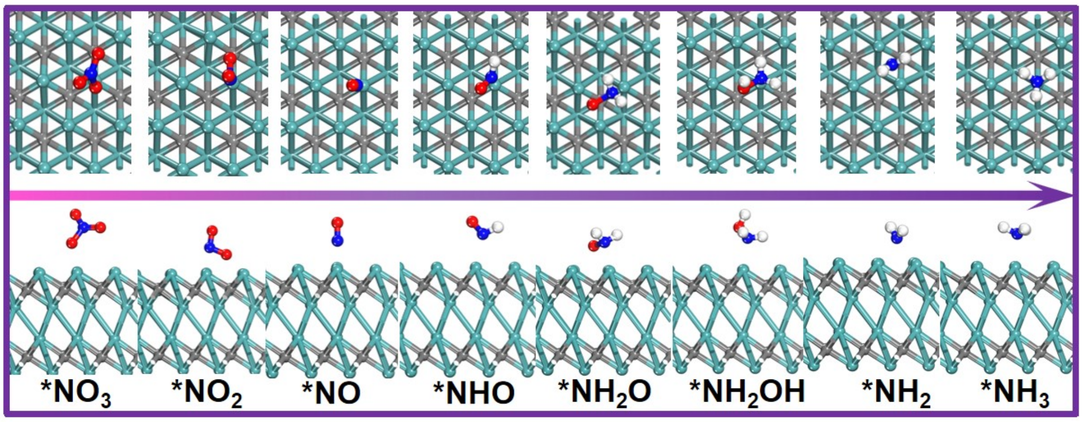

Fig. S11. Optimized structures of intermediate configurations through NHO hydrogenation pathway on Mo_2C.

Table S1. Comparison of the optimum NH_3 yield and FE_{NH3} for the recently reported state-of-the-art NRA electrocatalysts at ambient conditions.

Catalyst	**Electrolyte**	**NH_3 yield rate (mg h^{-1} cm^{-2})**	**FE_{NH3} (%)**	**Potential (V vs. RHE)**	**Ref.**
Fe-PPy SACs	0.1 M KOH （0.1 M KNO_3）	2.75	100	-0.7	[4]
Cu-PTCDA	1 M PBS （500 ppm KNO_3）	0.44	85.9	-0.4	[5]
CuCl_BEF	0.5 M Na_2SO_4 （100 mg/LNO_3^-）	1.82	44.7	-1.0	[6]
Fe_3O_4/SS	0.1 M NaOH (0.1 M $NaNO_3$)	10.15	91.5	-0.5	[7]
Fe-MoS_2	0.1 M Na_2SO_4 （0.1 M $NaNO_3$）	0.51	98	-0.48	[8]
$Cu_{10}Ce_{10}$	1 M KOH （10 mM NO_3^-）	16.83	98.43	-0.23	[9]
Poly-Cu_{14}cba	0.5 M K_2SO_4 （250 ppm NO_3^-）	2.84	90	-0.15	[10]
10Cu/TiO_{2-x}	0.5 M Na_2SO_4 （200 ppm $NaNO_3$）	1.94	81.34	−0.75 V	[11]
RuNi-MOF	0.1 M Na_2SO_4 （50 mg L^{-1} NO_3^-）	0.27	73	-1.2	[12]
Fe/Ni_2P	0.2 M K_2SO_4 50 mM KNO_3	4.17	94.3	−0.4 V	[13]
Mo_2C/RGO	0.5 M Na_2SO_4 （0.1 M NO_3^-）	**4.8**	**85.2**	**-0.6**	**This Work**

Supplementary references

[1]. P. Shen, G. Wang, K. Chen, J. Kang, D. Ma and K. Chu, *J. Colloid Interf. Sci.*, 2023, **629**, 563-570.

[2]. A. A. Peterson, *Energy Environ. Sci.*, 2010, **3**, 1311-1315.

[3]. P. Shen, X. Li, Y. Luo, Y. Guo, X. Zhao and K. Chu, *ACS Nano*, 2022, **16**, 7915-7925.

[4]. P. Li, Z. Jin, Z. Fang and G. Yu, *Energy Environ. Sci.*, 2021, **14**, 3522-3531.

[5]. G.-F. Chen, Y. Yuan, H. Jiang, S.-Y. Ren, L.-X. Ding, L. Ma, T. Wu, J. Lu and H. Wang, *Nat. Energy*, 2020, **5**, 605-613.

[6]. W. J. Sun, H. Q. Ji, L. X. Li, H. Y. Zhang, Z. K. Wang, J. H. He and J. M. Lu, *Angew. Chem., Int. Ed.*, 2021, **60**, 22933-22939.

[7]. X. Fan, L. Xie, J. Liang, Y. Ren, L. Zhang, L. Yue, T. Li, Y. Luo, N. Li, B. Tang, Y. Liu, S. Gao, A. A. Alshehri, Q. Liu, Q. Kong and X. Sun, *Nano Res.*, 2021, **15**, 3050–3055.

[8]. J. Li, Y. Zhang, C. Liu, L. Zheng, E. Petit, K. Qi, Y. Zhang, H. Wu, W. Wang and A. Tiberj, *Adv. Funct. Mater.*, 2022, **32**, 2108316.

[9]. L. Yang, J. Li, F. Du, J. Gao, H. Liu, S. Huang, H. Zhang, C. Li and C. Guo, *Electrochim. Acta*, 2022, **411**, 140095.

[10]. Y. M. Wang, J. Cai, Q. Y. Wang, Y. Li, Z. Han, S. Li, C. H. Gong, S. Wang, S. Q. Zang and T. C. Mak, *Angew. Chem., Int. Ed.*, 2022, **134**, e202114538.

[11]. X. Zhang, C. Wang, Y. Guo, B. Zhang, Y. Wang and Y. Yu, *J. Mater. Chem. A*, 2022, **10**, 6448-6453.

[12]. J. Qin, K. Wu, L. Chen, X. Wang, Q. Zhao, B. Liu and Z. Ye, *J. Mater. Chem. A*, 2022, **10**, 3963-3969.

[13]. R. Zhang, Y. Guo, S. Zhang, D. Chen, Y. Zhao, Z. Huang, L. Ma, P. Li, Q. Yang, G. Liang and C. Zhi, *Adv. Energy Mater.*, 2022, **12**, 2103872.